Solar Energy 274 (2024) 112572

Contents lists available at ScienceDirect

Solar Energy

journal homepage: www.elsevier.com/locate/solener

Natural ore filter cube decorated polypyrrole for effective thermal management and enhanced solar steam generator

Muhammad Sohail Asghar [a], Naila Arshad [a,b], Muhammad Sultan Irshad [a,b], Najah Alwadie [c], Xianbao Wang [a], Muhammad Atif Ali [b], Iftikhar Ahmed [d,*], Jinhua Li [a,*], Van Tan Tran [e], Vu Anh Doan [f], Van-Duong Dao [e,*], Jinming Guo [a,*]

[a] Ministry-of-Education Key Laboratory for Green Preparation and Application of Functional Materials, School of Materials Science and Engineering, Hubei University, 430062 Wuhan, China

[b] Collaborative Innovation Centre for Optoelectronic Science & Technology International Collaborative Laboratory of 2D, Materials for Optoelectronics Science and Technology of Ministry of Education Institute of Microscale Optoelectronics, Shenzhen University, Shenzhen 518060, China

[c] Department of Physics, College of Science, Princess Nourah bint Abdulrahman University, P. O. Box 84428, Riyadh 11671, Saudi Arabia

[d] Environmental and Public Health Department College of Health Sciences Abu Dhabi University, P.O. Box 59911, Abu Dhabi, United Arab Emirates

[e] Faculty of Biotechnology, Chemistry, and Environmental Engineering, Phenikaa University, Hanoi 100000, Viet Nam

[f] Faculty of Applied Chemistry Materials, School of Materials Science and Engineering, Hanoi University of Science and Technology, Hanoi 100000, Viet Nam

A R T I C L E I N F O

Keywords:
Natural ore filter cube
Polypyrrole
Thermal management
Solar steam generation
Freshwater

A B S T R A C T

Pursuing environmentally friendly and effective energy conversion technologies inspired research investigations into innovative materials and methods to generate solar steam. Herein, we demonstrate a novel methodology that leverages natural ore filter cubes anchored with polypyrrole (PPy) to enhance solar steam generation and effective thermal management via an in-situ polymerization technique. The natural ore filter cubes (NOFC) serve as a porous framework, offering a large surface area for excellent light absorption and hydrophilic water channels. Meanwhile, the PPy coating improves light absorption and effectively converts solar energy into thermal energy. The fabricated evaporator exhibits exceptional solar absorption capability (93 %), with a broad spectral response ranging from ultraviolet to near-infrared wavelengths (200–2500 nm). Moreover, the presence of PPy promotes an efficient evaporation rate (1.58 kg $m^{-2}h^{-1}$), resulting in rapid heating and vaporization of water under 1 kW m^{-2}. Natural ore filter cubes with PPy coating offer salt resistance, scalability, and environmental sustainability. Finally, this research presents an exciting way to improve solar steam-generating technology for water desalination and energy conversion applications.

1. Introduction

The freshwater shortage is posing a significant threat to both mankind and the ecosystem. This issue has been intensified by factors such as population growth, industrialization, and urbanization, which have further contributed to global warming and the lack of drinkable water [1–4]. While 97 % of our planet's surface is covered with water, the majority of it occurs in the form of seawater. Several technologies, such as reverse osmosis (RO) and multistage flash (MSF), were established to address water shortages by cleaning seawater [5,6] However, deploying these technologies requires sophisticated infrastructure, significant energy use, and continuous system maintenance. Solar power is an abundant source of renewable and sustainable energy that has the potential to meet all energy deficits across ecological and industrial sectors [7,8]. This is because the energy contained in the solar radiation that reaches the Earth's surface per hour exceeds the world's entire annual energy consumption [9–11]. In recent times, there has been an increasing emphasis on solar steam production as a sustainable energy solution for producing drinkable water from salty and wastewater sources [12,13]. This technology aims to mitigate water shortages while simultaneously preseving of the environmental hygiene. The effectiveness of any steam-generating system hinges on its ability to harness the

* Corresponding authors.
E-mail addresses: sohail.asghar673@gmail.com (M. Sohail Asghar), sultan.danish93@gmail.com (M. Sultan Irshad), wxb@hubu.edu.cn (X. Wang), dr.iftikhar.ahmed@live.fr (I. Ahmed), jinhua_li@hubu.edu.cn (J. Li), duong.daovan@phenikaa-uni.edu.vn (V.-D. Dao), guojinming@hubu.edu.cn, guojinming0123@126.com (J. Guo).

https://doi.org/10.1016/j.solener.2024.112572
Received 3 March 2024; Received in revised form 17 April 2024; Accepted 25 April 2024
Available online 30 April 2024

solar spectrum, its hydrophilicity, its thermal management, and its capacity to reject salt [14–17]. The photothermal conversion system has been meticulously designed to provide superior outcomes for thermal management, heat localization, and solar harvesting [18–20]. Till date, numerous solar-thermal conversion materials has been reported, such as metallic nanoparticles [21], semiconductors [22], and carbon-based materials [23,24], are deliberately designed to enhance the absorption of light. The fundamental function of the nanomaterial is to harvest the solar energy and release it in form of heat. Conversely, facilitating quick water access and retaining heat are two crucial roles that require aiding from advanced designs [25–27]. Hydrophilic surfaces with low thermal conductivity facilitate efficient water transportation and thermal management. Some examples of such substrates include wood sponges [28,29], polyurethane foam [30], and cellulose paper [31]. However, the manufacturing process for these solar steam generation (SSG) devices is quite complex. To mitigate the issues related to the scarcity of potable water, there is an urgent want for simple and efficient SSG systems that encompass all the essential components for convenient implementation on an industrial scale.

Natural ore filter materials have been used over the years as a cheap and efficient way in terms of cost to purify water against several waterborne diseases [32]. The small pore size filters out bacterial impurities while other merits of ceramic clay filters include portability, low cost, availability, and lightweight [33]. Moreover, they don't require additional energy input or alter water taste, unlike some chemicals [33]. The highly porous geometry facilitates efficient water transport. Although ceramic filters can filter most of the impurities from water, the produced water doesn't meet the standard the drinking water. Further, they can only treat mildly polluted water and cannot potentially treat sewage and wastewater efficiently [34]. Recently, conducting polymers have been recognized as effective photothermal materials for SSG systems. They manifest that broadband solar absorption has high stability, facile manufacturing, and economic feasibility [35]. Polypyrrole (PPy), is known as a highly stable conducting polymers characterized by its heterocyclic structure that allows for effective diffuse reflection and solar energy absorption [36,37]. It is widely used as a photothermal material by depositing on numerous hydrophilic substrates using various methods i.e., vapor phase polymerization, electropolymerization, and in-situ oxidative polymerization [38]. It has been reported to enhance the evaporation rate by photothermal conversion efficiency by omnidirectional absorption with minimum reflection to promote practical application [39]. However, the practical implementation of SSG designs suffers from the salt aching on the evaporator layer which decreases the conversion efficiency and deteriorates the endurance of photothermal layers [40]. The conventional techniques i.e., soaking and sonicating to remove the accumulated salt may cause surface degradation in form or cracks and remove the photothermal materials from the top layer [41]. Hence, a good SSG system should have the self-regenerating potential against salt accumulation under continuous operation for efficient water production.

Inspired by natural ore filter materials and the solar absorption potential of PPy, in-situ polypyrrole deposition on NOFC cubes has been developed NOFC@PPy for enhanced photothermal conversion efficiency, water transport, effective thermal management, and salt rejection, as illustrated in Figure 1. The NOFC@PPy achieved a surface temperature of 40.02 °C with a solar intensity of 1 kWm^{-2}, while effectively facilitating water transport to the top surface for rapid vapor escape. The in-situ polymerized NOFC exhibits enough black color, enabling it to efficiently absorb a broad spectrum of solar energy (93 %). These characteristics allow the in-situ polymerized NOFC evaporator to exhibit an evaporation rate of 1.58 kg $m^{-2}h^{-1}$ under 1 kWm^{-2} irradiation. It also demonstrates good endurance when subjected to long-term testing in seawater (3.5 wt%, 10.58 kg m^{-2} / 8 h @ one sun). The highly porous NOFC@PPy evaporator effectively repels the solid NaCl (1.2 g) by allowing the continuous escape of vapors through abundant water channels in a very short period (330 min). This avoids the buildup of salt within water transport channels. COMSOL Multiphysics (5.5) was used to simulate the soalr flux distribution and heat accumulation at the top surface using the heat transfer model and the heat conduction losses to the water below for the designed NOFC@PPy structure. The proposed solar evaporation structure shows the promise for practical application to satisfy individual demands which does not require any sophisticated

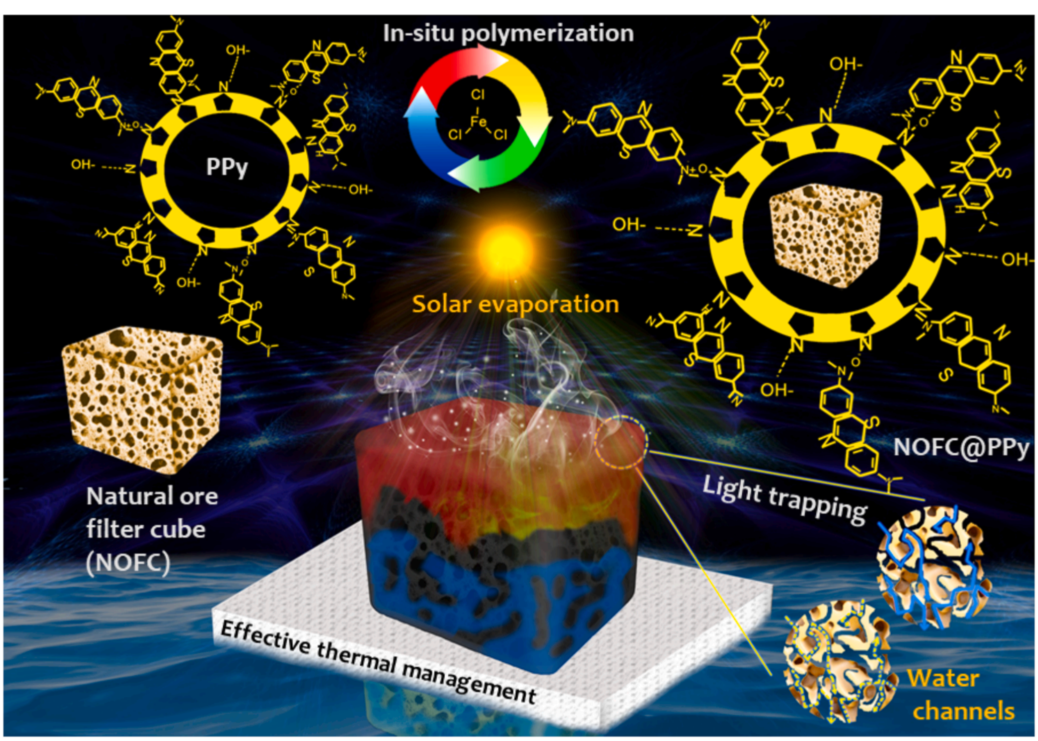

Figure 1. Schematic illustration of synthesis approach, and natural ore filter cube decorated polypyrrole for effective thermal management and enhanced solar steam generator.

installation infrastructure for potable water in remote areas.

2. Materials and methods

2.1. Materials

Natural ore filter cubes (NOFC) were obtained through Aladdin Industrial Corporation (Wuhan, China). Ammonium persulfate ($(NH_4)_2S_2O_8$) and pyrrole (C_4H_5N), water spray cans, ethanol (C_2H_5OH), and phytic acid ($C_6H_{18}O_{24}P_6$) had been offered by Macklin for in-situ polymerization of Natural ore filter cubes. Without performing any additional purifying process, all of the compounds obtained were used in the experiment.

2.2. In-situ polymerization of natural ore filter cubes

The PPy was anchored on the NOFCs cubes via facile in-situ polymerization technique, representing a straightforward and one-step method aimed at enhancing their solar absorption and photothermal conversion capabilities. In this procedure, 5.5 g of ammonium persulfate was mixed well in 10 mL of DI water, forming a colourless mixture designated as solution A. Concurrently, in another container, 1.68 mL pyrrole and 3.68 mL phytic acid (at 50 % concentration in water) were mixed with in isopropanol alcohol (10 mL) creating a dark brown mixture solution named as B. Afterwards, the prepared monomers were separately loaded into distinct spraying containers and sprayed in an lternating B-A-B-A order onto the surface of the NOFCs undergoing in-situ polymerization. This sequential spraying process was performed repetedly to ensure a consistent, even, and thoroughly polymerized coating. The iterations continued until the color of the NOFC cubes uniformly transitioned to a deep pitch-black shade. The mass of polymerized PPy on the NOFC cubes was determined by assessing the difference in mass before and after deposition, yielding a final value of 23 mg. The PPy polymerized NOFCs were positioned inside the polyethylene terephthalate (PET) in such a way that their bottoms were immersed inside bulk water. The PET foam bestows the floating potential to prepare a solar evaporation system.

The NOFC@PPy cubes-inspired solar evaporator exhibits salt-resistant and self-regenerating capabilities. Polypyrrole coatings can form dense and compact layers on surfaces. These coatings act as physical barriers that can inhibit the penetration of salt ions through the coating to the underlying substrate. This barrier effect helps protect the substrate from the damaging effects of salt exposure. Polypyrrole is capable of undergoing ion exchange processes, where it can selectively interact with certain ions. In the presence of salts, polypyrrole can adsorb and interact with ions without undergoing significant degradation or loss of its protective properties. The poly-pyrrole (PPy) coating on these filter cubes provides a protective barrier against salt accumulation owing to its diffuse surface texture, and oil film of PPy, preventing blockage and maintaining efficient water evaporation. Inspired by natural ore structures, these cubes also possess a unique self-regenerating property where excess salt is expelled during the evaporation process, allowing the cubes to continuously function without manual cleaning or maintenance.

2.3. Material characterization information

The anatomy and microstrcutures of the prepared NOFC and NOFC@PPy were scruntnized via field emission scanning electron microscope (FESEM, JSM7100F, JEOL, Tokyo, Japan). The elemental compositions and surface chemistry were assessed via X-ray photoelectron spectroscopy (XPS) (Thermo Fisher Scientific Escalab 250Xi, Waltham, MA, USA) utilizing a monochromatic source for X-ray production. The soalr absorbance was assessed by conducting UV–Vis abdosption test throughout the solar spectrum (200–2500 nm) using ultraviolet–visible near-infrared spectrophotometer (Shimadzu UV–vis-NIR UV-3600 double beam spectrophotometer, Kyoto, Japan). Surface temperature was recorded with an infrared camera (FLIR E4 Pro, Deer Park, NY, USA) incorporating two thermocouples for temperature measurement (K type, hand-held optical meter model). Fourier-transform infrared (FT-IR) spectroscopy was conducted with an FT-IR tester (Nicolet iS50, Waltham, MA, USA).

2.4. Solar steam generation setup

The time-dependent mass variations and evaporation test were performed employing a solar simulator (PLS-FX300HU) having capability to mimic a variety of sun intensities, reaching up to 6 kW m^{-2}. A typical optical filter in conjunction with a conventional 1.5 G amplitude modulation (AM) spectrum was applied. The NOFC@PPy solar evaporator was positioned in a petri dish containing water such that the bottom of the NOFC@PPy was submerged in the water and exposed to the simulated solar intensity. To track mass changes with respect to time, an advanced electronic balance (Mettler Toledo, ME204) was employed capable of measuring the changes with a high precision of 0.001 g. Under 1 kWm^{-2} solar irradiation, the whole experimental set up was exposed and waited for 30 min to maintain stability before testing to measure evaporation rates. The purifying potential of the NOFC@PPy was checked by using Inductively Coupled Plasma-Optical Emission Spectrometry (ICP-AES) to analyze the concentration of salt in simulated water and condensed water. The whole experimental set up was operated under ambient surroundings i.e., 18 °C and a humidity level of around 60 %. The Hand-Held Optical Meter Model was used to monitor surface temperatures.

3. Results and discussion

Natural ore filter cubes (NOFC) may improve seawater desalination filtration efficiency due to high porosity, surface area, and adsorption capability [42]. The selection of the PPy was made as it's an extensively studied conducting polymer with π-electron conjugation and shows excellent energy conversion ability with few toxicological concerns [43–47]. The polypyrrole coating on the NOFC@PPy permits the efficient capture of sunlight and its thermal energy conversion for continuous water evaporation. The porous structure ensures consistent transportation of water and high resistance to salt accumulation throughout the evaporation performance. The synthesized PPy nanoparticles were investigated for elemental and morphological analysis using microscopic methods, including FESEM, FTIR, and XPS. X-ray diffraction analysis reveals the amorphous nature of the PPy powder, as depicted in **Figure S1**. A wide peak was detected at around $2\theta = 25^{\circ}$. The broad peak is a distinctive feature of amorphous PPy and is caused by the scattering of PPy chains at the interplanar gap. **Figure S2** displays the Raman spectra of the PPy powder. The PPy Raman spectra showed two peaks appearing at 1345 cm^{-1} and 1558 cm^{-1}, which correspond to the D and G bands, respectively. The D band in PPy is associated with the stretching of the pyrrole ring, while the G band is related to the stretching of the C=C bond in the main backbone of PPy. The XPS scan of PPy (Figure 2a) manifests the existence of several elemental constituents i.e., C1s, N1s, O1s, and S2p, respectively. The observed highly resolved C1s spectrum is deconvulated into three sub-peaks indicating the multiple existing states into three distinct pieces with binding energies of 284.5, 286.3, and 288.4 eV. The first two components may be traced to the stable peak location of π-π interactions and (C=C) carboxyl group bonding state (C=O) in the polymeric chain, respectively. The peak appearing at 286.4 eV indicates the potential existence of bonding structures involving $C{=}N/{=}C{-}NH^{+}$ in between polymeric chains. Figure 2c demonstrates the splitting of the N1s spectrum into three sub-peaks appearing at distinct binding energies. The first signal positioned at 399.98 eV is ascribed to the existence of the –NH group in the pyrrolic ring. While, the subsequent elemental peaks set at 401.2 and 401.8 eV belong to the polaron state ($-NH^{+}-$) and bi-polaron $=NH^{+}-$ states,

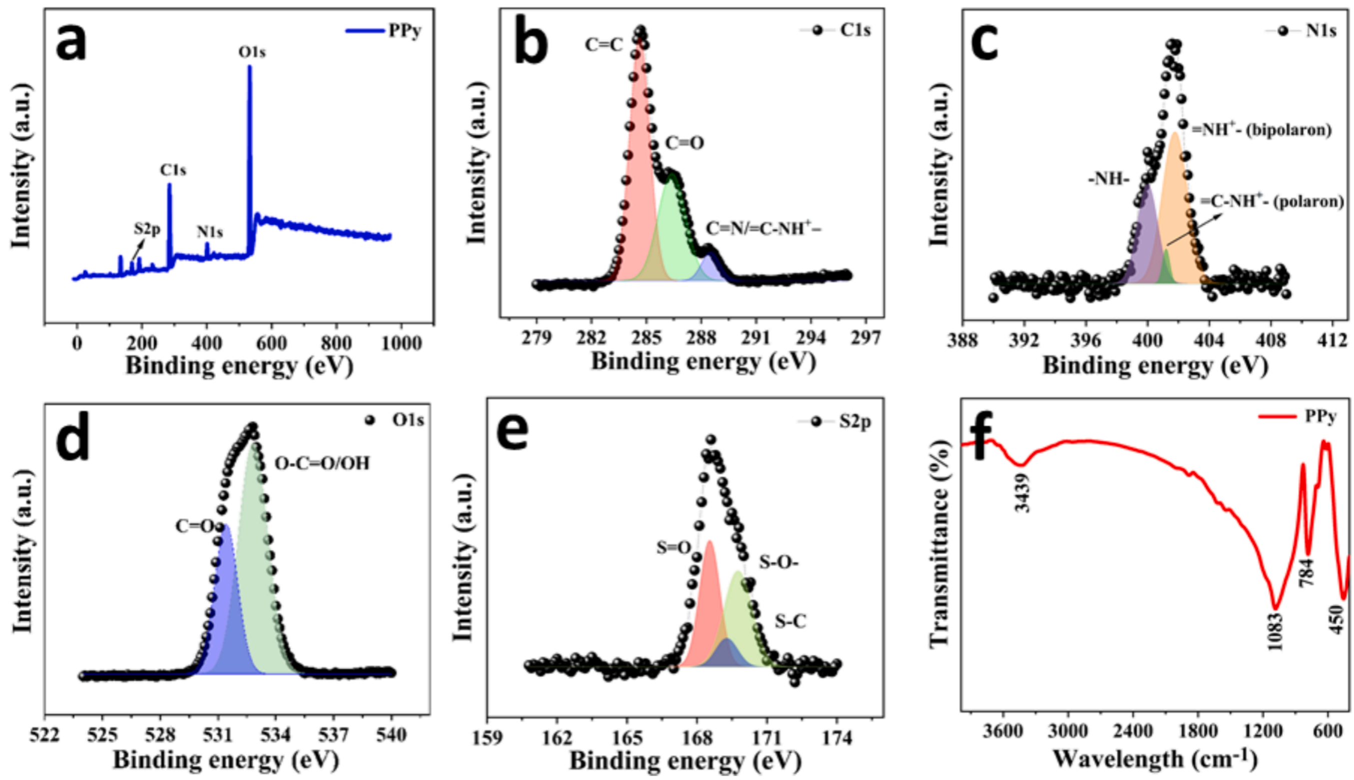

Figure 2. (a) XPS survey of PPy NPs. High-resolution XPS spectra of (b) C1s, (c) N1s, (d) O1s, and (e) S2p. (f) FTIR spectrum of PPy powder.

respectively. The XPS O1s spectrum into two components, indicating the multiple existing bonds at binding energy positions of 531.4, and 532.8 eV corresponding to the existence of C=O and O–C=O/OH bonds, respectively (Figure 2d). Furthermore, the XPS spectrum of the S2p spectrum may be decomposed into three distinct peaks at 168.6, 169.2, and 169.7 eV, representing the S=O, S-C, and S-O- species, respectively (Figure 2e). The FTIR spectra of PPy affirm the presence of multiple functional groups, as shown in Figure 2f. The absorption band at 407 cm^{-1} is associated with in-plane vibrations of =CH, whereas the peak at 784 cm^{-1} corresponds to the out-of-plane vibrations of=CH. The N–H in-plane deformation absorption of polypyrrole exhibits a significant peak of high intensity at 1083 cm^{-1}. The existence of a wide band at 3439 cm^{-1} in the polymeric network is explained by the OH groups stretching.

The facile in-situ polymerization technique involves a series of polymerization steps involving monomers that interact to form a polymer. PPy is a very stable conductive polymer because of its heterocyclic structure, which allows for light scattering within complex structures and good solar absorption which renders it a suitable material for solar-powered devices [36,37,48]. In-situ polymerization of natural ore filter cube substrate is one way to improve solar absorption and ultimate photothermal conversion through intrinsic defuse reflection of conductive PPy nanoparticles [48]. For this purpose, two solutions containing monomers, referred to as solutions A and B, were chosen. These solutions were applied sequentially to enable the in-situ polymerization of NOFC@PPy, as detailed in the material synthesis section. Figure 3a schematically illustrates the in-situ polymerization of NOFC to prepare solar evaporators for seawater desalination. The in situ synthesis of polypyrrole offers good scalability for large-scale production due to its straightforward and continuous process of polymerization, which can be easily scaled up by simply increasing the reaction volume. This method allows for the direct formation of polypyrrole within the desired substrate or medium, eliminating the need for subsequent purification steps and reducing material waste. This technique has room for improvement despite its scalability potential. Polymerized product homogeneity and quality might be challenging to control on a wider scale due to reaction circumstances or substrate qualities. Homogenous polymerization and product integrity at scale require consistent and efficient monomer delivery throughout the reaction volume. As production volumes increase, process parameters and reaction kinetics must be optimized and monitored, stressing the need for strong process design and control systems for in situ polypyrrole synthesis. The microstructural and morphological investigation of the bare NOFC and PPy anchored on the NOFC surface were performed employing FESEM. The FESEM images of bare NOFC and NOFC@PPy are shown in Figures 3b and 3c. Figure 3b shows the highly rough surface texture of NOFC with a porous surface which facilitates the water passage for steam and impedes salt resistance while a rough surface enhances solar absorption with minimum reflection. The uniform deposition of PPy on NOFC as a result of in-situ polymerization can be seen in Figure 3c. The homogeneous dispersion of PPy provides an overall compact and dense structure owing to successive polymerization. This PPy layer over NOFC enhances the ability to capture light by utilizing its inherent diffuse reflection property and localizing the solar flux to achieve a high surface temperature for evaporation. Besides, energy dispersive spectroscopy (EDS) was performed for the elemental mapping of the NOFC@PPy. The PPy-anchored NOFC affirms the existence and even distribution of primary elements C, N, O, and S, respectively, as shown in Figure 3(d-g).

The NOFC@PPy solar evaporator was fabricated employing a facile in-situ fabrication technique that bestows high porosity and hydrophilic water channels for continuous steam escape. Indeed, good hydrophilicity combined with optimum solar absorption plays a key role in developing an efficient and sustainable evaporation device. The hydrophilicity of the NOFC@PPy was assessed by performing the water absorption rate on the surface as seen in Figure 4(a-b). As obvious, the NOFC@PPy absorbs water quickly after ~ 0.1 s, showcasing a highly hydrophilic structure for excellent water uptake owing to interconnected water channels resulting in swift vapor escape. The effectiveness of SSGs heavily relies on their capability to harvest solar power with efficient conversion into heat via a photothermal mechanism for

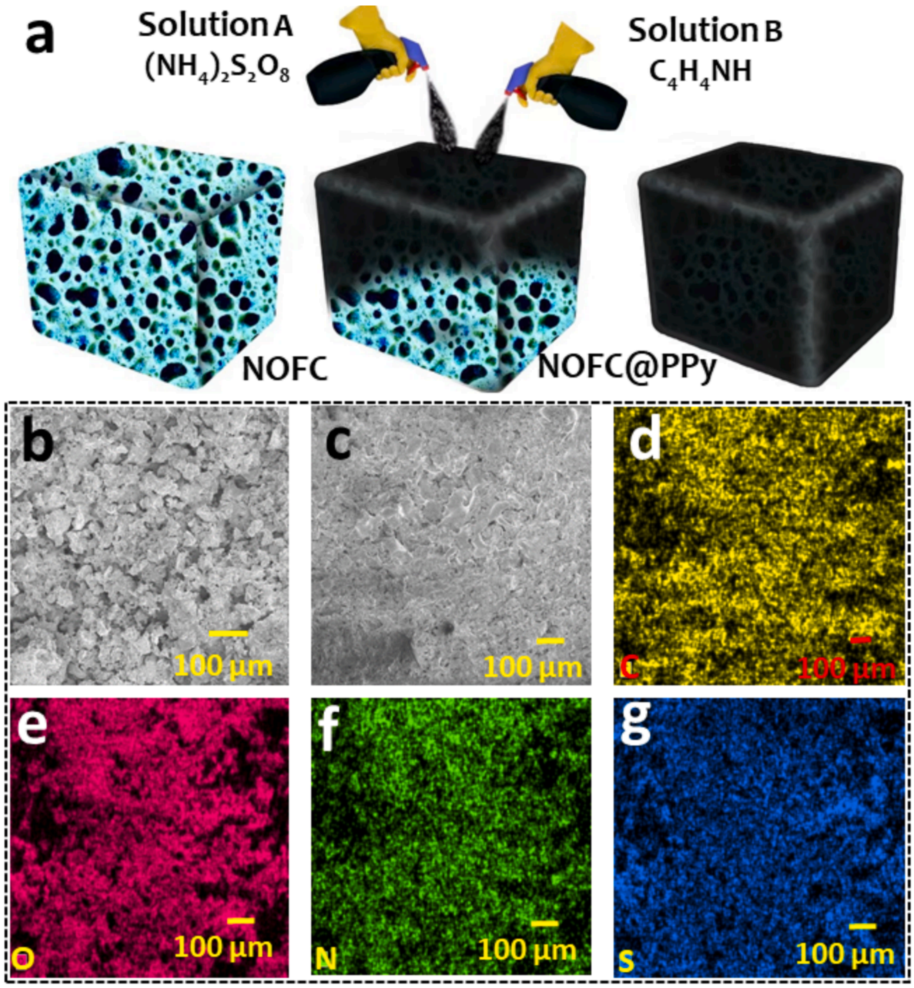

Figure 3. (a) Direct polymerization protocol for NOFC@PPy. (b-c) FESEM images of NOFC and NOFC@PPy. (d-g) EDS mapping of NOFC@PPy.

enhanced evaporation rate [5,49]. A salt-resistant system is developed that manifests the optimal capture of solar power and ultimate conversion into thermal energy. For this, the solar absorption of NOFC@PPy powder was quantified via UV–Vis-NIR spectroscopy, using an integrated sphere that covers the whole solar spectral length (200–2500 nm). The solar energy harvesting potential of NOFC@PPy demonstrates a good absorption rate of 93 % throughout a wide range of wavelengths computed employing the (1-T-R) formula, as shown in Figure 4c.

This is accomplished by the efficient capture of the incident light beams within the dense and rough surface texture of NOFC@PPy through diffused reflections within the black and porous surface which leads to multiple scattering of incident light and ultimate absorption within the structure. This results in increased solar absorption with a higher potential for energy conversion via good solar flux distribution throughout the surface. This efficient capacity for solar absorption leads to enhancement in surface temperature when exposed to incident solar irradiation. For this, three systems were aimed for better comparison (water, NOFC, and NOFC@PPy) are exposed to simulated one sun solar intensity (1 kWm^{-2}) to measure the time-dependent temperature elevation employing a thermocouple sensor probe and compare the surface temperature enhancement. The resulting time-dependent data of temperature rise for all three systems can be seen in Figure 4d. Under the simulated solar irradiation, the NOFC@PPy surface manifests a relatively quick rise in the surface temperature and achieves a thermal equilibrium within the first 10 min. Under constant irradiation for 1 h, the NOFC@PPy solar evaporator demonstrated a significant increase in surface temperature, reaching up to 40.02 °C manifesting good solabsorption and photothermal response. This temperature enhancement surpasses that of water and NOFC solar evaporators. Figure 4e shows the increase in NOFC@PPy surface temperature when exposed to different simulated irradiations (1, 2, 3 kWm^{-2}). It demonstrates that the in-situ polymerized NOFC temperature can rise as high as 60.3 °C under three sun, indicating effective heat retention and efficient thermal localization on the black surface. This excellent ability to concentrate thermal energy makes it an attractive structure for solar evaporation and thermal storage technologies.

Besides, the elevation in temperature with time was monitored employing an infrared (IR) camera for cross and top views when exposed to 1 sun irradiation. For this, the NOFC@PPy solar evaporators supported by PET foam were put in a petri dish containing water inside and irradiated by the simulated sunlight throughout the experiment. The time-dependent IR images of the cross and top surface can be seen in Figure 5(a-h) for the continuous monitoring of temperature elevation. Upon activating the solar simulator, the NOFC@PPy solar evaporator shows a quick response to solar light in terms of rapid surface temperature enhancement revealing the conversion of solar-thermal energy conversion on the upper coated layer.

As obvious, the top black surface of the NOFC@PPy solar evaporator shows a temperature rise of 36 °C in the first 10 min, exceeding the temperature of the surrounding environment. During the next 10-minute period, the top surface further manifests the temperature elevation up to 40 °C and attains the state of thermal equilibrium. Conversely, the cross-view of the NOFC@PPy solar evaporator demonstrates a much lower temperature in comparison to the upper surface, suggesting a

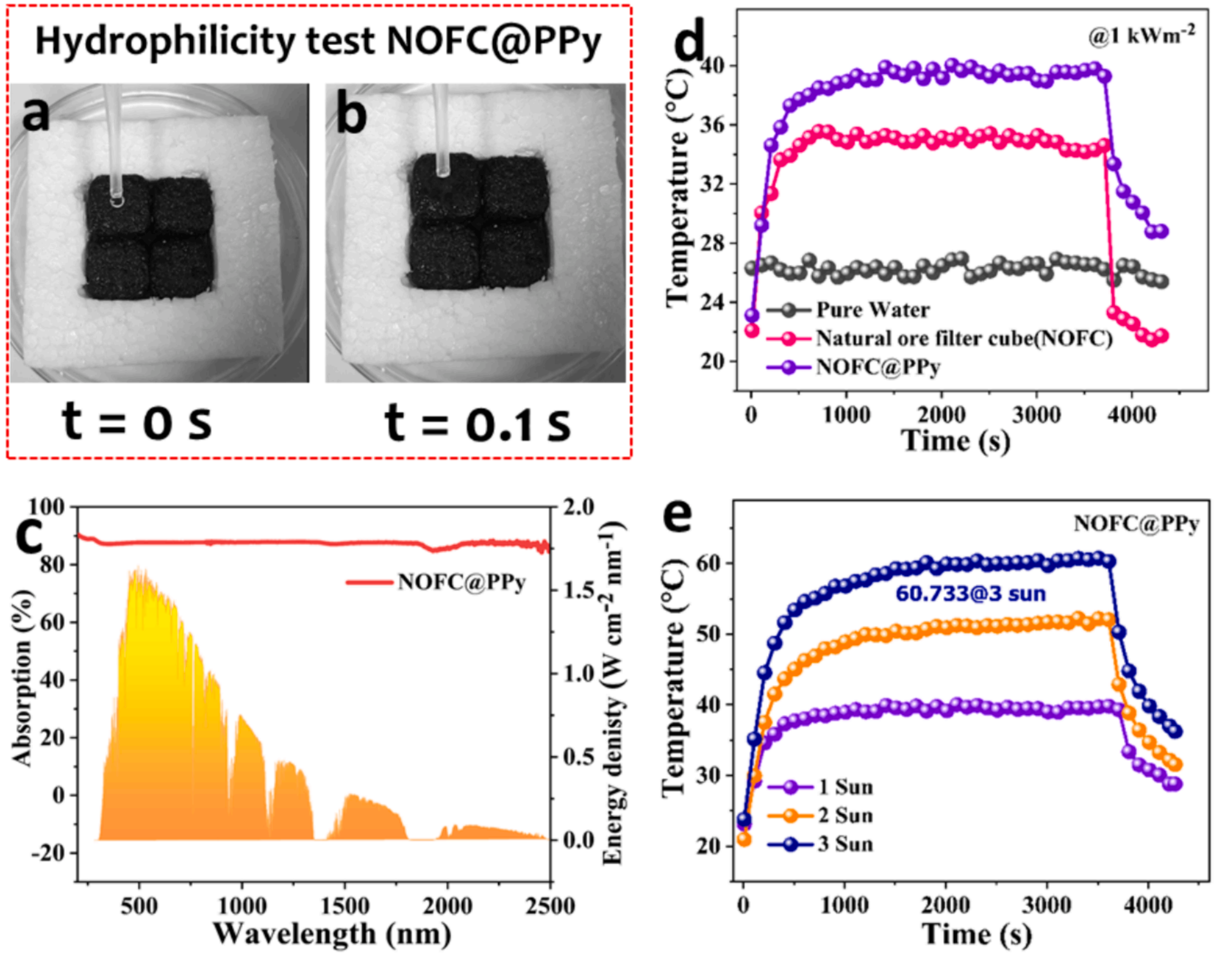

Figure 4. (a,b) Hydrophilic test of NOFC@PPy. (c) Solar absorption spectra of NOFC@PPy. (d) The time-dependent temperature rise of pure water, NOFC, and NOFC@PPy solar evaporators. (e) The time-dependent temperature rise of NOFC@PPy solar evaporator under multiple simulated irradiations.

deficiency in downward heat conduction and efficient thermal insulation. As a consequence, there was efficient concentration of heat on the upper surface. An ideal "thermal localization" was achieved and an effective evaporation rate was subsequently promoted by the NOFC@PPy solar evaporator, which displayed a combination of asymmetrical thermal conductivity with effective photothermal transformation. More importantly, the heat transfer module for the in-situ polymerized natural ore filter cube (NOFC@PPy) is designed which replicate the actual geometry and experimental conditions of evaporation performances using COMSOL Multiphysics 6.0. This comprises the factors i.e., temperature of water and surfaces, material selection, and thermal conductivity. The heat transfer module encompasses an extensive range of functionalities for examining heat models and the impacts of heat flux. The generated symmetry accurately reproduces the parametric presentation of IR pictures for the NOFC@PPy evaporation structures. The upper black layer of NOFC@PPy acts as a thermal barrier resulting in a noticeable difference in temperature across the contact. Figure 5(i-l) shows the developed heat-transferring geometries corresponding to the IR images of NOFC@PPy exhibiting good heat localization over the top resulting in an elevation of surface temperature (41.02 °C). The simulated geometry reveals good thermal distribution on the top surface of NOFC@PPy while an increased thermal gradient can be seen from the cross view resulting in a sudden temperature decrease towards the lower surface [49]. The simulated heat models extenuate the precise correlation with the designed solar evaporator in terms of thermal distribution over the top and bottom surfaces. Hence, key factors taken into account for the design of an effective solar evaporation device are the capturing of solar power, maximum solar power conversion into thermal energy into heat, and the good hydrophilic of the device for high vapor generation.

The basic mechanism of the solar-powered steam generation structure is the efficient localization of heat at the interface greatly enhanced by the rugged and integrated dark surface texture of the NOFC@PPy to facilitate achieving a high evaporation rate. Optimal solar absorption and little thermal conduction lead to enhanced interfacial thermal localization and exceptional sun-to-vapor conversion efficiency. The NOFC@PPy solar evaporator is illustrated in Figure 6a under 1 kWm^{-2}. Figure 6b shows NOFC@PPy solar evaporator is placed inside a dome-shaped glass jar to collect the condensing water that is evaporated under simulated solar intensity. As clear, the condensing glass is fully covered with hot water vapors which ultimately condenses to produce fresh water. To measure the evaporation performance of NOFC@PPy under 1 kW m^{-2}, we conducted a comparison study of three different systems: pure water, NOFC, and NOFC@PP-based solar evaporators for 1 h. The high surface temperature facilitates rapid evaporation, resulting in a high evaporation rate. The in-situ polymerized solar evaporator achieved a maximum mass of 1.58 kg m^{-2}, which was much greater compared to other evaporation systems i.e., pure water (0.18 kg m^{-2}) and NOFC (1.05 kg m^{-2}), as seen in Figure 6b. The salt-resistant NOFC@PPy solar evaporator's evaporation rate was also measured over a range of sun intensities. Figure 6c shows that under 3 k W m^{-2}, the highest observed mass change was 4.63 kg m^{-2}. This high mass change leads to a high evaporation rate and ultimately high evaporation efficiency. The evaporation rates of the developed three systems were

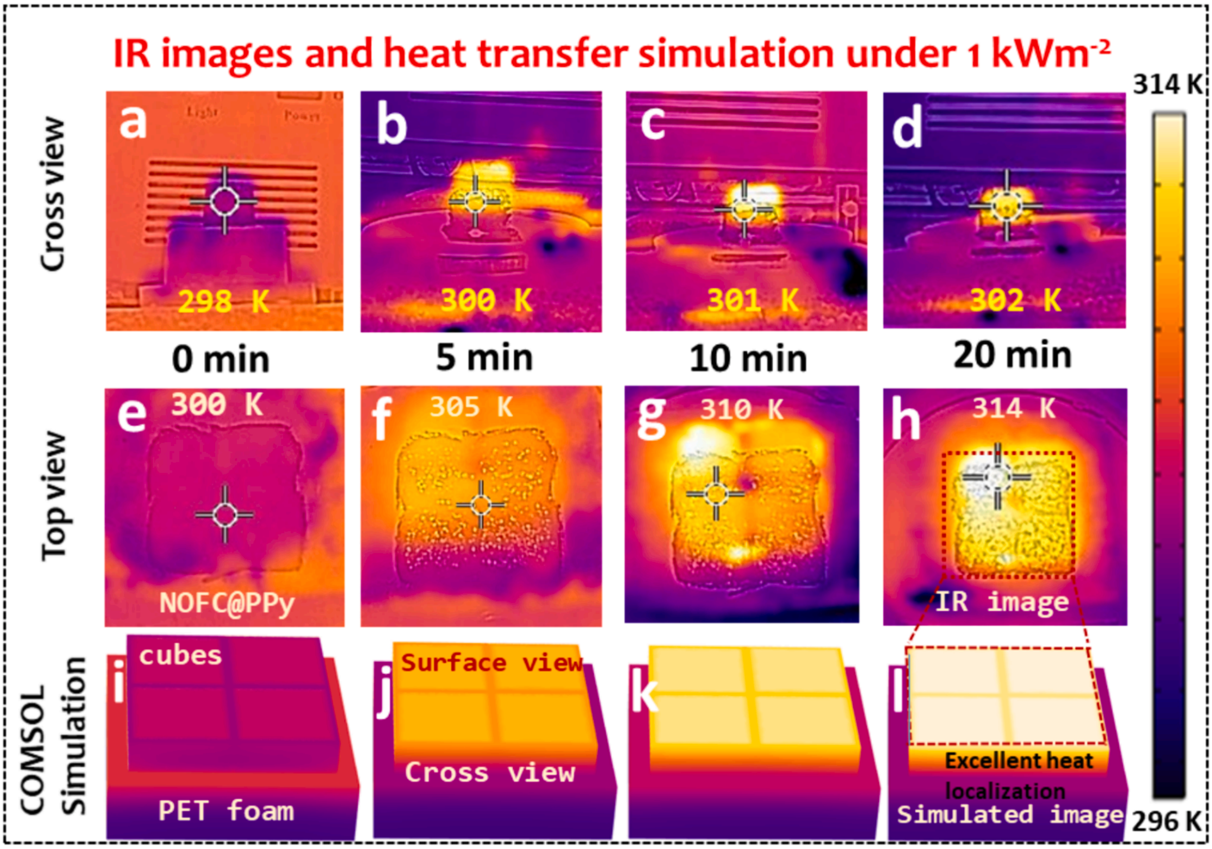

Figure 5. Surface temperature distribution via cross-view (a-d), and (e-h) top view of NOFC@PPy solar evaporator under solar irradiance captured by IR camera. (i-l) Heat transfer simulations of NOFC@PPy solar evaporator under one sun.

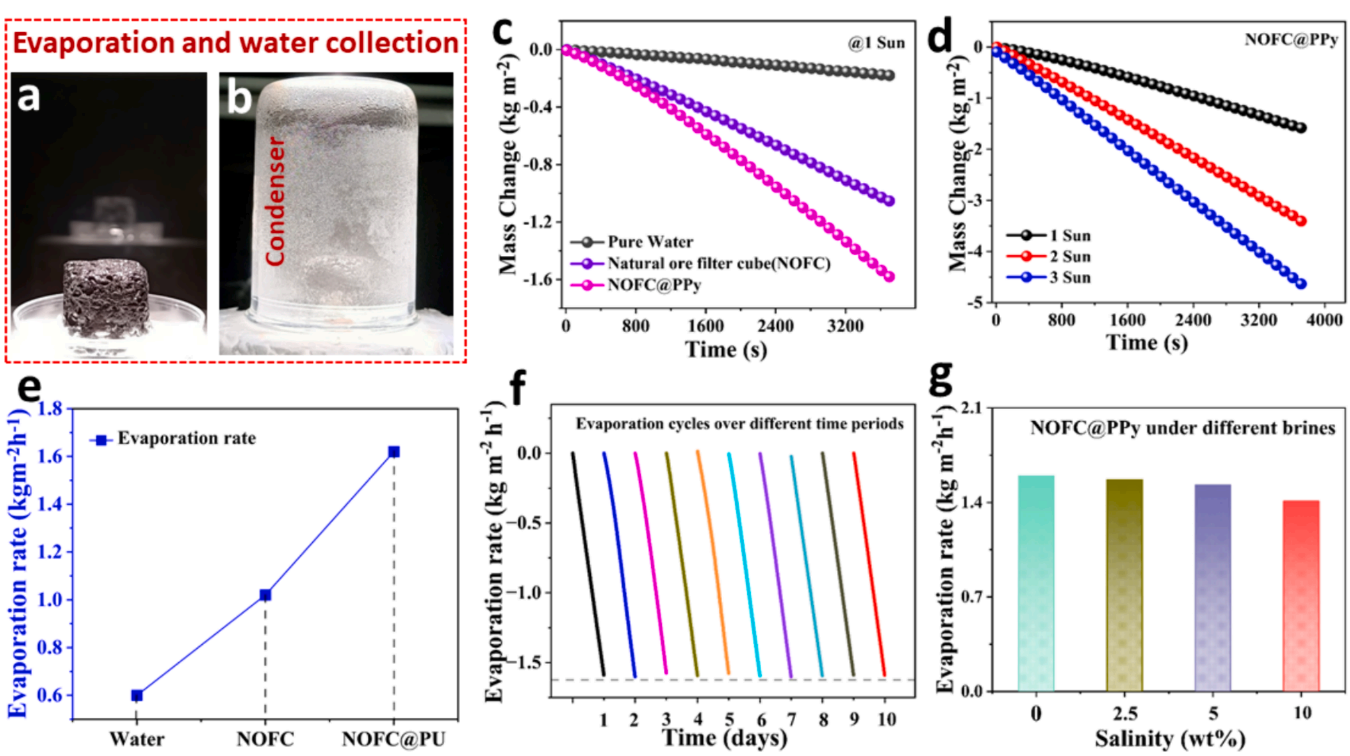

Figure 6. (a-b) Real-time demonstration of NOFC@PPy solar evaporator, and its vapor condensing. (c-d) Mass changes of different solar evaporators including NOFC@PPy solar evaporator under one sun and multiple solar intensities. (e) Evaporation rates of different solar evaporators including NOFC@PPy. (f) Evaporation rate curves of NOFC@PPy solar evaporator continuous ten cycles over different periods under one sun irradiation. (g) Evaporation of NOFC@PPy solar evaporator under different brines concentrations i.e., (0, 2.5, 5, 10, and 20 wt%).

calculated excluding the dark evaporation rate and presented in Figure 6d. The NOFC@PPy solar evaporator has a maximum evaporation rate of 1.58 kg $m^{-2}h^{-1}$, which is significantly higher than pure water and NOFC-based solar evaporators. The solar-thermal conversion efficiency (η_{evap}) of the NOFC@PPy solar evaporator was measured by the following equation [50–54].

$$\eta_{evap} = \frac{\dot{m}_v h_{LV}}{q_i} \quad (1)$$

$$h_{LV} = \lambda + C\Delta T \quad (2)$$

Where $m_{\cdot v}$ shows the evaporation rate (1.58 kg $m^{-2}h^{-1}$) excluding the evaporation rate under no light, h_{LV} is the liquid-to-vapor phase change enthalpy, q_{solar} is simulated sunlight, here assumed to be 1 kW m^{-2}. Where ʎ indicates latent heat of evaporation, C shows the specific heat capacity of water (4.2 kJ kg^{-1} K^{-1}), and △T is water temperature variations.

The experimental environmental temperature was 18 ± 1 °C and with 60 % humidity while performing experiments. From (i-ii) equations, NOFC@PPy solar evaporator achieved 87 % solar-thermal conversion efficiency subtracting optical and heat losses. The consistency of evaporation performance in terms of cyclic stability and durability for NOFC@PPy solar evaporator was quantitatively assessed by performing the evaporation test under 1 kWm^{-2} for 10 days, as shown in Figure 6e. The NOFC@PPy solar evaporator maintains a consistent evaporation rate without any noticeable change in slope over time, demonstrating the exceptional stability of the system. Besides, the NOFC@PPy solar evaporator was tested under multiple simulated salt solutions i.e., pure water, 2.5, 5, 10, and 20 wt% brine solutions to evaluate its resistance to salt and restoration capacities while sustaining smooth evaporation rates, as seen in Figure 6f. As expected, the developed salt-resistant solar evaporator maintained a good evaporation rate with negligible discrepancy even under highly concentrated brine solution revealing its potential to perform under intense conditions which entails it as an efficient and sustainable system for large-scale seawater desalination applications. The evaporation rate of the NOFC@PPy solar evaporator was compared with the previously developed state-of-the-art solar evaporation systems and presented in the form of **Table S1**. The NOFC@PPy shows the superior performance among them ascribed to its rough black surface and porosity of the material which enables efficient water absorption and vapor escape. The polypyrrole coating enhances light absorption and heat localization, promoting efficient energy conversion at the water–air interface. The system's ability to convert solar irradiation into thermal energy efficiently contributes to its high steam generation rate. The incorporation of PET foam around the NOFC@PPy cubes influences heat transfer efficiency and water evaporation kinetics by allowing vertical water transfer. Hence, optimized structural design minimizes heat loss and maximizes water exposure to sunlight.

Solar energy is an environmentally friendly and renewable energy source, that is used in the desalination process of seawater. Due to the elevated salt concentration in seawater (3.5 wt% NaCl), the water channels in evaporation structures are prone to blockage during extended operations. Introducing new thin evaporation structures without sacrificing thermal insulation is one of the efficient strategies proposed to address this problem. Several effective methods have been proposed to address this problem lately, one of which is the introduction

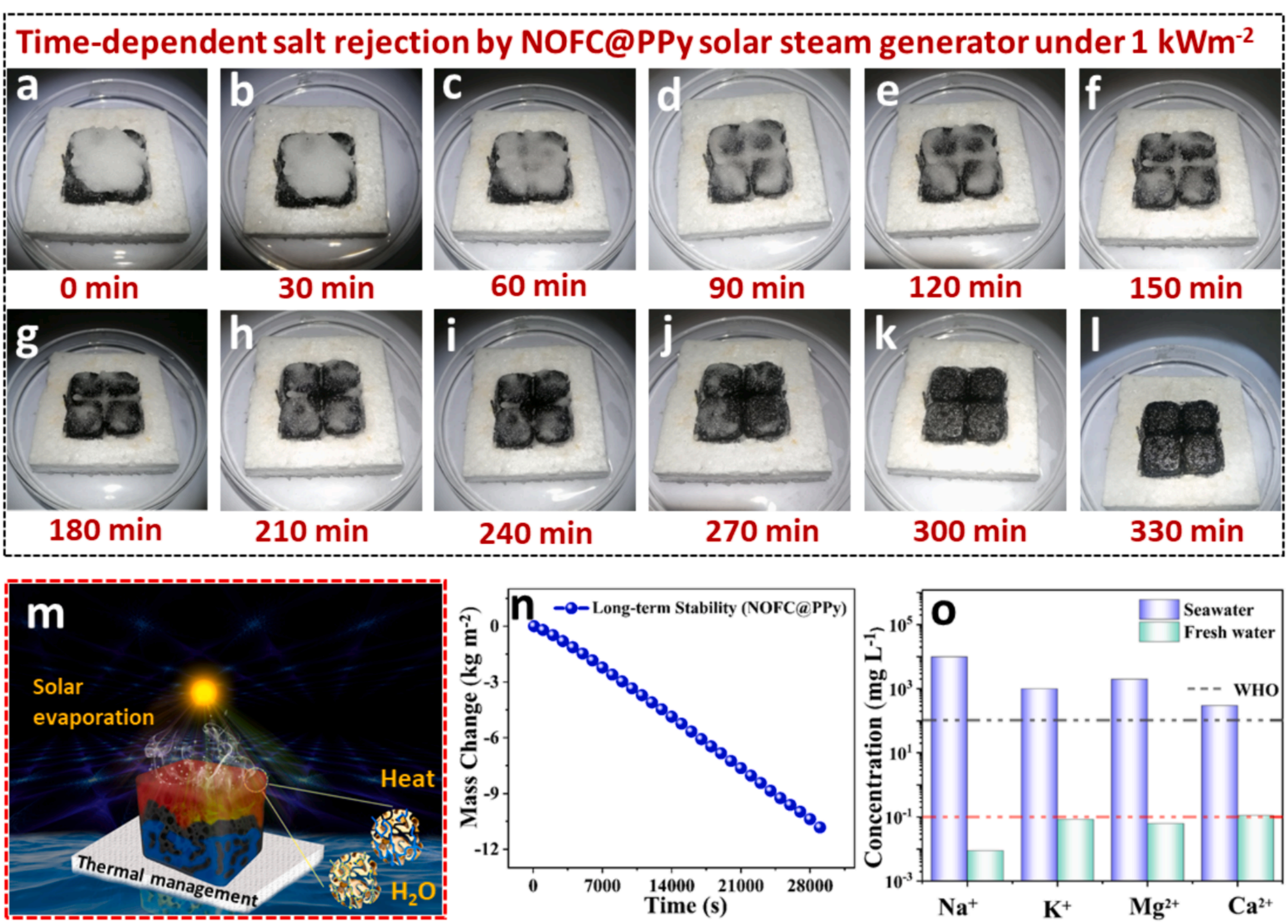

Figure 7. (a-l) Represents the salt-dissolution capability of NOFC@PPy solar evaporator during continuous performance under one sun solar irradiance. (m) Schematic illustration of heat accumulation, and open porous structure of NOFC@PPy for salt-dissolution. (n) Continuous solar evaporation performance of NOFC@PPy solar evaporator under one sun solar irradiance. (o) ICP-OES examination of source and condensed water.

of new thin evaporation structures at the cost of thermal insulation. The buildup of salt hinders the maximization of evaporation efficiency. The salt-resistant and salt-rejection capabilities of the solar-powered NOFC@PPy were assessed by placing the NOFC@PPy solar evaporator in a petri filled with simulated seawater containing 3.5 wt% NaCl. It was then exposed to 1 sun irradiation for several hours while 0.85 g of solid NaCl were placed over its surface, as seen in Figure 7(a-l). Over a period of 5.5 h of continuous irradiation, the NOFC@PPy solar evaporator completely expelled 0.85 g of solid NaCl, showing excellent self-regeneration ability with consistent and uninterrupted steam production. The device's capacity to reject salt and regenerate is attributed to the cross-linked and aligned porous structure. Salt ions will travel from an area of high concentration to an area of low concentration due to the potential gradient formed by the various concentrations in the two locations. The solid NaCl dissolves when vapor flows steadily, allowing it to move through the top surface into the bulk water via aligned porous symmetry and avoid the buildup of salt.

Hence, the suggested approach has significant potential for extensive use in large-scale industrial seawater desalination. Figure 7 m schematically illustrates the NOFC@PPy solar evaporator which efficiently captures the solar light via rough and black surface texture and generates vapors through aligned water channels with good thermal management. However, a major challenge faced by evaporation structures is the buildup of salt or structural deformation when used continuously for an extended time, which greatly impacts the evaporation rate and efficiency of the devices. NOFC@PPy solar evaporator was continuously run for 8 h under one sun to observe smooth evaporation without any structural deformation, as shown in Figure 7n. The NOFC@PPy solar evaporator demonstrates a consistent mass change of 10.82 kg m^{-2} throughout an 8-hour period of exposure to one sun illumination. The purification potential of the condensed water was checked against the nano-filtration potential for primary metal ions rejection using inductively coupled plasma-optical emission spectrometry (ICP-OES). Figure 7o shows the concentration of primary metal ions (Na^+, K^+, Mg^{2+}, and Ca^{2+}) in simulated water and condensed form. The ion concentration in the condensed water is substantially lower than the level established by the World Health Organization for drinking water. Polypyrrole (PPy) coatings exhibit promising salt and heavy metal rejection potential owing to their unique physicochemical properties. The conductive nature of PPy films enables ion exclusion mechanisms, making them effective barriers against salt ions during filtration processes. Furthermore, the surface charge and porosity of PPy coatings can be tailored to selectively repel or adsorb heavy metal ions based on electrostatic interactions. The presence of functional groups within the PPy structure allows for specific binding sites for heavy metal ions, enhancing their removal efficiency. Overall, the tunable properties of Polypyrrole coatings make them attractive candidates for applications requiring selective rejection of salts and heavy metals in various filtration and purification systems. Hence, we have created a NOFC@PPy solar evaporator that may be used for practical applications without surface deterioration and is suitable for industrial-level installation to produce freshwater.

4. Conclusion

In conclusion, this study offers an innovative way to improve solar steam generation and thermal management by combining NOFC coated with PPy. The NOFC framework offers a porous structure with ample surface area for effective light absorption and facilitates hydrophilic water channels, while the PPy coating further enhances light absorption and promotes the efficient conversion of solar energy into thermal energy. The developed evaporator shows excellent solar absorption efficiency of 93 % over a wide spectral range from 200 to 2500 nm. It produces a high evaporation rate of 1.58 kg $m^{-2}h^{-1}$ under 1 kW m^{-2}, enabling fast water heating and vaporization. Furthermore, the inherent properties of NOFC and PPy, including resistance to salt, recyclability, scalability, and environmental sustainability, underscore the potential for widespread application in various fields such as water desalination, sterilization, and renewable energy production. Overall, our study proposes a highly promising approach to advancing solar steam generation technology, offering considerable benefits for both environmental preservation and technological innovation.

CRediT authorship contribution statement

Muhammad Sohail Asghar: Conceptualization, Writing – original draft. **Naila Arshad:** Conceptualization, Writing – original draft, Writing – review & editing. **Muhammad Sultan Irshad:** Conceptualization, Formal analysis, Validation, Writing – review & editing. **Najah Alwadie:** Formal analysis. **Xianbao Wang:** Visualization. **Muhammad Atif Ali:** Visualization. **Iftikhar Ahmed:** Funding acquisition, Investigation, Supervision. **Jinhua Li:** Funding acquisition, Investigation, Project administration, Supervision. **Van-Duong Dao:** Supervision, Visualization. **Jinming Guo:** Conceptualization, Funding acquisition, Investigation, Project administration, Resources, Supervision, Validation.

Declaration of Competing Interest

The authors declare that they have no known competing financial interests or personal relationships that could have appeared to influence the work reported in this paper.

Acknowledgment

This work was financially supported by the National Natural Science Foundation of China (Grant No. 52001117). This work is also supported by Princess Nourah bint Abdulrahman University Researchers Supporting Project number (PNURSP2024R478), Princess Nourah bint Abdulrahman University, Riyadh, Saudi Arabia. This work was financially supported by the Vietnam National Foundation for Science and Technology Development (NAFOSTED) (grant number 103.02-2021.106).

Appendix A. Supplementary data

Supplementary data to this article can be found online at https://doi.org/10.1016/j.solener.2024.112572.

References

[1] M.S. Irshad, N. Arshad, M.S. Asghar, Y. Hao, M. Alomar, S. Zhang, J. Zhang, J. Guo, I. Ahmed, N. Mushtaq, M.A.K.Y. Shah, L. Noureen, S. Wageh, O.A. Al-Hartomy, A. Kalam, V.D. Dao, H. Wang, X. Wang, H. Zhang, Advances of 2D-enabled photothermal materials in hybrid solar-driven interfacial evaporation systems toward water-fuel-energy crisis, 2304936, Adv. Funct. Mater. (2023) 1–30, https://doi.org/10.1002/adfm.202304936.

[2] C. Song, M.S. Irshad, Y. Jin, J. Hu, W. Liu, Arabic-dome-inspired hierarchical design for stable and high-efficiency solar-driven seawater desalination, Desalination 544 (2022) 116125, https://doi.org/10.1016/j.desal.2022.116125.

[3] N. Arshad, M.S. Irshad, M.S. Asghar, M. Alomar, J. Tao, M.A.K.Y. Shah, X. Wang, J. Guo, S. Wageh, O.A. Al-Hartomy, et al., 2D MXenes embedded perovskite hydrogels for efficient and stable solar evaporation, Glob. Challenges (2023) 2300091.

[4] A.M. Saleque, S. Ma, A.K. Thakur, R. Saidur, T.K. Han, M.I. Hossain, W. Qarony, Y. Ma, R. Sathyamurthy, Y.H. Tsang, MXene/MnO_2 nanocomposite coated superior salt-rejecting biodegradable luffa sponge for efficient solar steam generation, Desalination 554 (2023) 116488.

[5] M.S. Irshad, X. Wang, A. Abbas, F. Yu, J. Li, J. Wang, T. Mei, J. Qian, S. Wu, M. Q. Javed, Salt-resistant carbon dots modified solar steam system enhanced by chemical advection, Carbon n. y. 176 (2021) 313–326.

[6] A.M. Saleque, S. Saha, M.N.A.S. Ivan, S. Ahmed, T.I. Alam, S.U. Hani, Y.H. Tsang, Reduced graphene oxide/$TiTe_2$ quantum dot coated waste face mask recycled for highly efficient solar steam generation, Sol. Energy Mater. Sol. Cells 253 (2023) 112232, https://doi.org/10.1016/j.solmat.2023.112232.

[7] X. Liu, D.D. Mishra, X. Wang, H. Peng, C. Hu, Towards highly efficient solar-driven interfacial evaporation for desalination, J. Mater. Chem. A (2020).

[8] X. Li, X. Min, J. Li, N. Xu, P. Zhu, B. Zhu, S. Zhu, J. Zhu, Storage and recycling of interfacial solar steam enthalpy, Joule 2 (2018) 2477–2484, https://doi.org/10.1016/j.joule.2018.08.008.

[9] V. Badescu, Modeling solar radiation at the earth's surface, SpringerVerlag, Berlin/Heidelb, 2008.

[10] M. He, H. Dai, H. Liu, Q. Cai, Y. Liu, L. Wang, X. Qin, J. Yu, High-performance solar steam generator based on polypyrrole-coated fabric via 3D macro- and microstructure design, ACS Appl. Mater. Interfaces 13 (2021) 40664–40672, https://doi.org/10.1021/acsami.1c11802.

[11] M. He, H. Liu, L. Wang, X. Qin, J. Yu, One-step fabrication of a stretchable and anti-oil-fouling nanofiber membrane for solar steam generation, Mater. Chem. Front. 5 (2021) 3673–3680.

[12] Y. Wang, X. Wu, T. Gao, Y. Lu, X. Yang, G.Y. Chen, G. Owens, H. Xu, Same materials, bigger output: A reversibly transformable 2D–3D photothermal evaporator for highly efficient solar steam generation, Nano Energy 79 (2021) 105477, https://doi.org/10.1016/j.nanoen.2020.105477.

[13] H. Liu, J. Gu, Y. Liu, L. Yang, L. Wang, J. Yu, X. Qin, Reconfiguration and self-healing integrated Janus electrospinning nanofiber membranes for durable seawater desalination, Nano Res. 16 (2023) 489–495.

[14] V.-D. Dao, N.H. Vu, H.-L.-T. Dang, S. Yun, Recent advances and challenges for water evaporation-induced electricity toward applications, Nano Energy 85 (2021) 105979, https://doi.org/10.1016/j.nanoen.2021.105979.

[15] R. Djellabi, L. Noureen, V.-D. Dao, D. Meroni, E. Falletta, D.D. Dionysiou, C. L. Bianchi, Recent advances and challenges of emerging solar-driven steam and the contribution of photocatalytic effect, Chem. Eng. J. 431 (2022) 134024, https://doi.org/10.1016/j.cej.2021.134024.

[16] N. Arshad, M.S. Irshad, M. Alomar, J. Guo, M.S. Asghar, N. Mushtaq, M.A. K. Yousaf, U. Ghazanfar, M. Shah, X. Wang, Y. Hao, L.T. Do, V.-D. Dao, H. Wang, Z. Ouyang, H. Zhang, Exploring perovskite oxide for advancing salt-resistant photothermal membranes and reliable thermoelectric generators, Chem. Eng. J. 475 (2023) 146200, https://doi.org/10.1016/j.cej.2023.146200.

[17] V.-D. Dao, N.H. Vu, H.-S. Choi, All day Limnobium laevigatum inspired nanogenerator self-driven via water evaporation, J. Power Sources 448 (2020) 227388, https://doi.org/10.1016/j.jpowsour.2019.227388.

[18] V.-D. Dao, An experimental exploration of generating electricity from nature-inspired hierarchical evaporator: The role of electrode materials, Sci. Total Environ. 759 (2021) 143490, https://doi.org/10.1016/j.scitotenv.2020.143490.

[19] R. Li, F. Yao, Y. Xu, S. Bai, Z. Jia, Q. Lin, Optimizing the charge carrier dynamics of thermal evaporated TexSe1-x Films for high-performance short-wavelength infrared photodetection, Adv. Funct. Mater. 34 (2024) 2307005.

[20] M. He, H. Dai, L. Wang, X. Qin, J. Yu, Facile fabrication of polydopamine nanosphere-decorated fabric for solar steam generation, Text. Res. J. 92 (2022) 3451–3461.

[21] M. Gao, P.K.N. Connor, G.W. Ho, Plasmonic photothermic directed broadband sunlight harnessing for seawater catalysis and desalination, Energy Environ. Sci. 9 (2016) 3151–3160, https://doi.org/10.1039/C6EE00971A.

[22] M.S. Irshad, X. Wang, M. Abbasi, N. Arshad, Z. Chen, Z. Guo, L. Yu, J. Qian, J. You, T. Mei, Semiconductive, Flexible MnO_2 NWs/Chitosan Hydrogels for Efficient Solar Steam Generation, ACS Sustain. Chem. Eng. 9 (n.d.) 3887–3900. https://doi.org/10.1021/acssuschemeng.0c08981.

[23] X. Han, L. An, Y. Hu, Y. Li, C. Hou, H. Wang, Q. Zhang, Ti3C2 MXene-derived carbon-doped TiO2 coupled with g-C3N4 as the visible-light photocatalysts for photocatalytic H2 generation, Appl. Catal. B Environ. 265 (2020) 118539, https://doi.org/10.1016/j.apcatb.2019.118539.

[24] A.M. Saleque, A.K. Thakur, R. Saidur, M.I. Hossain, W. Qarony, M.S. Ahamed, I. Lynch, Y. Ma, Y.H. Tsang, rGO coated cotton fabric and thermoelectric module arrays for efficient solar desalination and electricity generation, J. Mater. Chem. A 12 (2024) 405–418, https://doi.org/10.1039/D3TA04715F.

[25] Y. Wang, X. Wu, B. Shao, X. Yang, G. Owens, H. Xu, Boosting solar steam generation by structure enhanced energy management, Sci. Bull. 65 (2020) 1380–1388, https://doi.org/10.1016/j.scib.2020.04.036.

[26] A.M. Saleque, S. Ahmed, M.N.A.S. Ivan, M.I. Hossain, W. Qarony, P.K. Cheng, J. Qiao, Z.L. Guo, L. Zeng, Y.H. Tsang, High-temperature solar steam generation by MWCNT-HfTe2 van der Waals heterostructure for low-cost sterilization, Nano Energy 94 (2022) 106916, https://doi.org/10.1016/j.nanoen.2022.106916.

[27] A.M. Saleque, M.N.A.S. Ivan, S. Ahmed, Y.H. Tsang, Light-trapping texture bio-hydrogel with anti-biofouling and antibacterial properties for efficient solar desalination, Chem. Eng. J. 458 (2023) 141430, https://doi.org/10.1016/j.cej.2023.141430.

[28] Y. Lu, D. Fan, Z. Shen, H. Zhang, H. Xu, X. Yang, Design and performance boost of a MOF-functionalized-wood solar evaporator through tuning the hydrogen-bonding interactions, Nano Energy 95 (2022) 107016, https://doi.org/10.1016/j.nanoen.2022.107016.

[29] A.M. Saleque, S. Ma, S. Ahmed, M.I. Hossain, W. Qarony, Y.H. Tsang, Solar driven interfacial steam generation derived from biodegradable luffa sponge, Adv. Sustain. Syst. 5 (2021) 2000291, https://doi.org/10.1002/adsu.202000291.

[30] M.S. Irshad, X. Wang, N. Arshad, M.Q. Javed, T. Shamim, Z. Guo, H.R. Li, J. Wang, T. Mei, Bifunctional in-situ polymerized nanocomposites for convective solar desalination and enhanced photo-thermoelectric power generation, Environ. Sci. Nano (2022).

[31] N. Hu, Y. Xu, Z. Liu, M. Liu, X. Shao, J. Wang, Double-layer cellulose hydrogel solar steam generation for high-efficiency desalination, Carbohydr. Polym. 243 (2020) 116480.

[32] G.M. Shayo, E. Elimbinzi, G.N. Shao, C. Fabian, Severity of waterborne diseases in developing countries and the effectiveness of ceramic filters for improving water quality, Bull. Natl. Res. Cent. 47 (2023) 113.

[33] L.J. Westholm, E. Repo, M. Sillanpää, Filter materials for metal removal from mine drainage—a review, Environ. Sci. Pollut. Res. 21 (2014) 9109–9128.

[34] M.A. Al-Ghouti, M.A. Al-Kaabi, M.Y. Ashfaq, D.A. Da'na, Produced water characteristics, treatment and reuse: A review, J. Water Process Eng. 28 (2019) 222–239.

[35] F. Wang, Z. Hu, Y. Fan, W. Bai, S. Wu, H. Sun, Z. Zhu, W. Liang, A. Li, Salt-rejection solar absorbers based on porous ionic polymers nanowires for desalination, Macromol. Rapid Commun. 42 (2021) 2000536, https://doi.org/10.1002/marc.202000536.

[36] M.S. Irshad, N. Arshad, J. Zhang, C. Song, N. Mushtaq, M. Alomar, T. Shamim, V.-D. Dao, H. Wang, X. Wang, H. Zhang, Wormlike Perovskite Oxide Coupled with Phase-Change Material for All-Weather Solar Evaporation and Thermal Storage Applications, Adv. Energy Sustain. Res. n/a (n.d.) 2200158. 10.1002/aesr.202200158.

[37] Z. Wei, N. Arshad, M.S. Irshad, M. Idrees, I. Ahmed, H. Li, H.H. Qazi, M. Yousaf, L. A. Alshahrani, Y. Lu, A scalable prototype by in situ polymerization of biodegradables, cross-linked molecular mode of vapor transport, and metal ion rejection for solar-driven seawater desalination, Crystals 11 (2021), https://doi.org/10.3390/cryst11121489.

[38] U. Ahmed, M. Alizadeh, N. Abd Rahim, S. Shahabuddin, M.S. Ahmed, A.K. Pandey, A comprehensive review on counter electrodes for dye sensitized solar cells: a special focus on Pt-TCO free counter electrodes, Sol. Energy 174 (2018) 1097–1125.

[39] J. Wang, T. Shamim, N. Arshad, M.S. Irshad, M.N. Mushtaq, C. Zhang, M. Yousaf, L. A. Alshahrani, M. Akbar, Y. Lu, In situ polymerized Fe2O3@ PPy/chitosan hydrogels as a hydratable skeleton for solar-driven evaporation, J. Am. Ceram. Soc. 105 (2022) 5325–5335.

[40] F. Wang, Y. Su, Y. Li, D. Wei, H. Sun, Z. Zhu, W. Liang, A. Li, Salt-resistant photothermal materials based on monolithic porous ionic polymers for efficient solar steam generation, ACS Appl. Energy Mater. 3 (2020) 8746–8754.

[41] G. Liu, T. Chen, J. Xu, G. Yao, J. Xie, Y. Cheng, Z. Miao, K. Wang, Salt-Rejecting Solar Interfacial Evaporation, Cell Reports Phys. Sci. 2 (2021) 100310, https://doi.org/10.1016/j.xcrp.2020.100310.

[42] H. Cheng, H. Lin, H. Huo, Y. Dong, Q. Xue, L. Cao, Continuous removal of ore floatation reagents by an anaerobic–aerobic biological filter, Bioresour. Technol. 114 (2012) 255–261.

[43] S. Zhang, J. Chen, J. Zheng, X. Chen, H. Xu, F.I.T. Petrescu, L.M. Ungureanu, Y. Li, G. Shi, A simple polypyrrole/polyvinylidene fluoride membrane with hydrophobic and self-floating ability for solar water evaporation, Nanomaterials 12 (2022) 859.

[44] Z. Wang, Y. Yan, X. Shen, C. Jin, Q. Sun, H. Li, A wood–polypyrrole composite as a photothermal conversion device for solar evaporation enhancement, J. Mater. Chem. A 7 (2019) 20706–20712.

[45] W. Huang, G. Hu, C. Tian, X. Wang, J. Tu, Y. Cao, K. Zhang, Nature-inspired salt resistant polypyrrole–wood for highly efficient solar steam generation, Sustain. Energy Fuels 3 (2019) 3000–3008.

[46] Y. Xu, J. Wang, F. Yu, Z. Guo, H. Cheng, J. Yin, L. Yan, X. Wang, Flexible and efficient solar thermal generators based on polypyrrole coated natural latex foam for multimedia purification, ACS Sustain. Chem. Eng. 8 (2020) 12053–12062, https://doi.org/10.1021/acssuschemeng.0c03164.

[47] Y. Li, J. Fan, R. Wang, W. Shou, L. Wang, Y. Liu, 3D tree-shaped hierarchical flax fabric for highly efficient solar steam generation, J. Mater. Chem. A 9 (2021) 2248–2258, https://doi.org/10.1039/D0TA09570B.

[48] X. Zhou, F. Zhao, Y. Guo, B. Rosenberger, G. Yu, Architecting highly hydratable polymer networks to tune the water state for solar water purification, eaaw5484, Sci. Adv. 5 (2019), https://doi.org/10.1126/sciadv.aaw5484.

[49] M.S. Irshad, N. Arshad, X. Wang, H.R. Li, M.Q. Javed, Y. Xu, L.A. Alshahrani, T. Mei, J. Li, Intensifying solar interfacial heat accumulation for clean water generation excluding heavy metal ions, and oil emulsions, Sol. RRL n/a (n.d.). 10.1002/solr.202100427.

[50] Z. Lei, X. Sun, S. Zhu, K. Dong, X. Liu, L. Wang, X. Zhang, L. Qu, X. Zhang, Nature inspired MXene-decorated 3D honeycomb-fabric architectures toward efficient water desalination and salt harvesting, Nano-Micro Lett. 14 (2022) 1–16.

[51] C. Gao, J. Zhu, Z. Bai, Z. Lin, J. Guo, Novel ramie fabric-based draping evaporator for tunable water supply and highly efficient solar desalination, ACS Appl. Mater. & Interfaces 13 (2021) 7200–7207.

[52] Y. Zhu, G. Tian, Y. Liu, H. Li, P. Zhang, L. Zhan, R. Gao, C. Huang, Low-cost, unsinkable, and highly efficient solar evaporators based on coating MWCNTs on nonwovens with unidirectional water-transfer, Adv. Sci. 8 (2021) 2101727.

[53] L. Song, P. Mu, L. Geng, Q. Wang, J. Li, A novel salt-rejecting linen fabric-based solar evaporator for stable and efficient water desalination under highly saline water, ACS Sustain. Chem. & Eng. 8 (2020) 11845–11852.

[54] Q. Qi, Y. Wang, W. Wang, X. Ding, D. Yu, High-efficiency solar evaporator prepared by one-step carbon nanotubes loading on cotton fabric toward water purification, Sci. Total Environ. 698 (2020) 134136.